Efficient coupling of heat-flow and electro-optical models for simulation of dynamics in high-power broad-area semiconductor lasers

M. Radziunas*, J. Fuhrmann*, A. Zeghuzi†, H.-J. Wünsche*†, Th. Koprucki*, H. Wenzel†, and U. Bandelow*
*Weierstrass Institute (WIAS), Mohrenstrasse 39, 10117 Berlin, Germany. Email: Mindaugas.Radziunas@wias-berlin.de
†Ferdinand-Braun-Institut, Leibniz Institut für Höchstfrequenztechnik, Gustav-Kirchhoff-Str. 4, 12489 Berlin, Germany.

***Abstract*—The aim of the work presented here is an efficient coupling of a heat flow (HF) model defined on multiple vertical-lateral subdomains and a dynamic electro-optical (EO) model acting in the longitudinal-lateral plane. Due to the different time scales, we propose an iterative coupling of the dynamic EO and static HF models. HF-solver calculates temperature and thermally-induced refractive index change within the active region. The EO-solver exploits these distributions and provides time-averaged field intensities, quasi-Fermi potentials, carrier densities, and bias current. All these time-averaged distributions are used again by the HF-solver for generation of the heat source.**

High-power (HP) edge-emitting broad-area semiconductor lasers (BALs), see Fig. 1(a), are important light sources due to their numerous applications. Accurate modeling and simulation of HP BALs are critical for improving their performance or for the evaluation of novel design concepts. Proper treatment of the self-heating-induced changes of the refractive index plays a crucial role in defining the essential emission characteristics of BALs operated in continuous-wave (CW) mode.

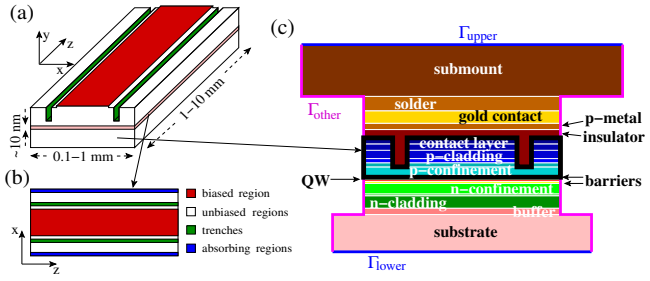

Fig. 1. Schematic representation of an edge-emitting broad-area laser (a), its active zone where the TW model is defined (b), and the transversal cross-section (c), where the thermal equations and the carrier flow equations (smaller black-framed region) are solved.

Electro-optical model: For modeling the nonlinear dynamics in BALs, we use a 2(space)+1(time) dimensional traveling wave (TW) model [1], [2] and the EO-solver BALaser [3] developed at WIAS Berlin. In this model, we take into account only the optical field and carrier dynamics within the thin active zone of the laser along the lateral and longitudinal coordinates x and z, see Fig. 1(b). A set of effective model parameters represents the influence of the vertical device structure. In the computational domain, we distinguish different areas according to the positions of the electrical contacts, etched trenches, or unbiased regions. The following TW equations govern the spatiotemporal dynamics of the slowly varying complex amplitudes of the counter-propagating optical fields $E^+(z,x,t)$ and $E^-(z,x,t)$:

$$\begin{aligned}&\left[\tfrac{1}{v_g}\partial_t \pm \partial_z + \tfrac{i}{2\bar{n}k_0}\partial_x^2\right] E^\pm = -i\beta E^\pm - i\kappa E^\mp + F_{sp}^\pm,\\ &E^+(0,x,t) = \sqrt{R_0}E^-(0,x,t) + \mathcal{O}(x,t),\\ &E^-(l,x,t) = \sqrt{R_l}E^+(l,x,t) + (1-R_l)[\mathcal{F}E^+](x,t).\end{aligned} \tag{1}$$

Here, v_g, κ, $k_0 = 2\pi/\lambda_0$, $\bar{n}$, and $F_{sp}^\pm$ are the group velocity of light, the field coupling factor in the presence of Bragg gratings, the free-space central wavenumber (λ_0: central wavelength), the reference refractive index, and the Langevin noise term, respectively. Parameters R_0 and R_l are the field intensity reflection coefficients of the facets of the diode at $z = 0$ and $z = l$ (l: the length of the BAL), whereas the function $\mathcal{O}(x,t)$ and the linear operator $\mathcal{F}$ represent an optical injection and a feedback from an external cavity, respectively [2]. At the lateral borders of the (sufficiently broad) computational domain periodic conditions are imposed. The complex propagation factor $\beta(z,x,t)$ accounts for linear and nonlinear (two-photon) absorption [4], an initially induced refractive index profile (etched trenches), material gain, and refractive index. The last two factors depend on the local carrier density $N(z,x,t)$ and take into account nonlinear gain compression [4] and material gain dispersion. The diffusive rate equation governs the dynamics of the carrier densities. To determine carrier diffusion and injected current (pump) at the active zone, we simultaneously solve the carrier spreading problem in the lateral/vertical (x/y) cross-sections [black-framed region in Fig. 1(c)] of the BAL device [5]. For more details on the model and typical diode parameters, see Refs. [1], [2], [4]. Finally, the factor $\beta(z,x,t)$ contains also a thermally-induced contribution n_T to the refractive index [6]. It is initially ignored in the case of pulsed operation of the laser, or adjusted using the procedure discussed in this work in the CW bias case.

Thermal model: A HF model for BALs should take into account the heat spreading in the whole device and, in general, is given by a (3+1)-dimensional heat conduction equation. However, due to the strongly differing time scales and limited computing resources, such a model is not applicable for the study of the thermal-optoelectronic dynamics in BALs. For this reason, we introduce two main simplifications. First, since the characteristic distances in the longitudinal (z) and transversal (x/y) directions differ by at least ten times, we neglect the heat diffusion in z direction, which allows considering the following dynamic heat conduction equation for each z:

$$c_L(x,y,z)\partial_t T = \nabla_{x,y}\cdot(\kappa_L(x,y,z)\nabla_{x,y})T + h(x,y,z,t).$$

978-1-5386-5599-3/18/$31.00 ©2018 IEEE

Here, the temperature distribution $T(x, y, z, t)$ satisfies the boundary conditions $\kappa_L \partial_n T = (T_{HS} - T)/r_{th}$ at the heat sink (upper or lower border of the domain), and $\partial_n T = 0$ at the remaining outer bounds, and preserves the continuity of the flux $\kappa_L \partial_n T$ at the interfaces between different materials, see Fig. 1(c). Coefficients c_L and κ_L are thermal capacity and conductivity, respectively, whereas h is the heat source depending on the field intensity P, quasi-Fermi potential φ, carrier density N, and current flow j, and should be separately generated at each considered z. Our second simplification is motivated by the huge difference in the time scales of opto-electronic and thermal processes. For this reason, within up to several nanosecond long transients we ignore the temperature evolution and exploit the time-averaged temperature $\bar{T}(x, y, z)$ instead. The static HF problem for $\bar{T}$ at each z reads as

$$\nabla_{x,y} \cdot (\kappa_L(x, y, z) \nabla_{x,y} \bar{T}(x, y, z) + \bar{h}(x, y, z) = 0, \qquad (2)$$

where $\bar{h}$ is the time-averaged heat source generated by the EO-solver during the previous few-ns transient simulation. For the numerical solution of Eq. (2), we use the toolkit pdelib [7] developed at WIAS Berlin. The numerical method is based on a finite volume space discretization, resulting in a sparse linear system of equations $A_h T_h = -h_h$ (A_h, h_h, T_h: discrete approximations of the differential operator, source, and temperature, respectively) which is solved via the LU factorization $A_h = L_h U_h$ into easily invertible upper and lower triangular factors, s.t. $T_h = -U_h^{-1} L_h^{-1} h_h$ [8]. Since the differential operator in Eq. (2) is linear and most of the considered BALs have a single or only a few different cross-sections, the same LU factorization can be applied w.r.t. multiple source functions h_h corresponding to different values of z. For typical laser structures, the calculation time required by the HF-solver does not exceed 1-2 minutes (compare to 10-30 minutes needed for standard 1-ns long transient simulations of the same BALs by the EO-solver). Typical calculated heat distributions within the lateral-vertical cross-section and within the active layer of the HP-BAL device are shown in Fig. 2(a).

Coupling of the HF- and EO-solvers: The EO- and HF-solvers are self-consistently coupled using the following iterative procedure. First of all, we perform ≥ 5 ns transient simulations of the BAL with the dynamic EO-solver using (if present) the temperature and the related refractive index distributions $\bar{T}(x, z)$ and $\bar{n}_T(x, z)$. If these distributions are not available, we neglect $\bar{n}_T$ and set $\bar{T}$ to a fixed heatsink temperature T_{HS}. Next, as the result of EO simulations, we get time-averaged distributions $\bar{P}(x, z)$, $\bar{N}(x, z)$, $\bar{\varphi}(x, z)$, and $\bar{j}(x, z)$. All these functions together with the additionally supplied vertical optical mode intensity profile $\Phi(y)$ are used for construction of the (time-averaged) heat source function $\bar{h}(x, y, z)$. Finally, the static HF-solver solves numerically Eq. (2) for the heat source $\bar{h}$ defined before. From the obtained 3-dimensional distribution $\bar{T}(x, y, z)$, we construct 2-dimensional functions $\bar{T}(x, z)$ and $\bar{n}_T(x, z)$ in the active layer and proceed to the first step of this iterative procedure. Panels (b)-(d) of Fig. 2 illustrate how this iterative procedure works. When first initiating the EO-solver, the considered BAL is switched off, whereas the distributions $\bar{T}$ and $\bar{n}_T$ are set to constants T_{HS} and 0, respectively. Near- and far-fields averaged over the last 2 ns of the first 5 ns transient simulations are shown by upper black curves in Fig. 2(b) and (c). In the absence of a thermally induced refractive index

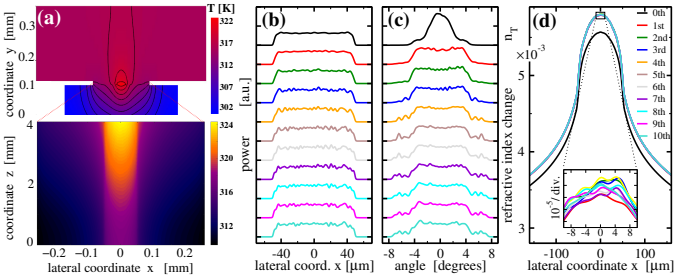

Fig. 2. Simulation results for 4 mm-long and 90 μm-wide HP-BAL device with $\sim$ 13 W emission power. (a): calculated temperature distribution within the lateral-vertical cross-section (top) and within the active layer (bottom). (b), (c), and (d): evolution of the time-averaged near-fields, far-fields, and thermally-induced refractive index change profiles $n_T(x)$ at the front facet during the iterative application of EO- and HF-solvers. Solid black curves correspond to the initial iteration step where temperature distribution was not yet accounted for in EO solver.

profile n_T, the far-field divergence is relatively small, see the upper curve in panel (c). The HF-solver exploits time-averaged distributions calculated by the EO-solver for the definition of $\bar{T}$ and $\bar{n}_T$, see the black curve in panel (d). Next, the EO-solver during the consequent 5 ns transient calculations accounts for the previously defined $\bar{T}$ and $\bar{n}_T$, whereas the HF-solver is using the heat sources specified by the just corrected time averaged distributions. Panel (d) shows how the initial correction slightly enhances the profile of $\bar{n}_T$, whereas the following iterations imply only small additional deviations (order 10^{-5}) of $\bar{n}_T$. The near- and, especially, far- fields change further during this iterative procedure. Whereas the flat-top of the near fields [panel (b)] exhibit small-amplitude oscillations, the far fields [panel (c)] indicate growing emission around $\pm 6°$. After approximately seven iterations (40 ns after switching on the laser), these distributions converge.

In conclusion, we discussed an efficient coupling of the dynamic EO- and the static HF-solvers for BALs. The calculation time used by the HF solver usually is less than 5% of the time required by the EO solver. The application of the HF-solver allows a self-consistent estimation of the temperature distribution and the thermal lensing within the active zone of the device, which is crucial for a proper simulation of the emission from CW HP-BALs by the EO-solver.

Acknowledgment

This work is supported by the German Federal Ministry of Education and Research contract 13N14005 as part of the EffiLAS/HotLas project and by the EUROSTARS Project E!10524 HIP-Lasers.

References

[1] M. Radziunas and R. Čiegis, *Math. Model. and Anal.*, 19:627-644, 2014

[2] M. Radziunas, *The Int. J. of High Perform. Comp. Appl.*, First online December 23, 2016, doi: 10.1177/1094342016677086.

[3] "BALaser: a software tool for simulation of dynamics in Broad Area semiconductor Lasers," http://www.wias-berlin.de/software/BALaser.

[4] A. Zeghuzi et al., *Opt. and Quantum Electron.*, **50**, 88, 2018.

[5] M. Radziunas et al., *Optical and Quantum Electronics*, **49**, 332, 2017.

[6] S. Rauch et al., *Appl. Phys. Lett.* **110**(26), 263504, 2017.

[7] J. Fuhrmann, T. Streckenbach et al., http://pdelib.org.

[8] T. A. Davis, UMFPACK V4.3, ACM TOMS, **30**(2) 196 - 199, 2004.